





# The Key RuV=O Intermediate of Site-Isolated Mononuclear Water Oxidation Catalyst Detected by in Situ X-ray Absorption Spectroscopy

## Journal Article

### Author(s):

Lebedev, Dmitry ; Pineda-Galvan, Yuliana; Tokimaru, Yuki; Fedorov, Alexey ; Kaeffer, Nicolas ; Copéret, Christophe ; Pushkar, Yulia

### Publication date:

2018-01

### Permanent link:

<https://doi.org/10.3929/ethz-b-000231836>

### Rights / license:

[In Copyright - Non-Commercial Use Permitted](#)

### Originally published in:

Journal of the American Chemical Society 140(1), <https://doi.org/10.1021/jacs.7b11388>

# The Key $\text{Ru}^{\text{V}}=\text{O}$ Intermediate of Site-Isolated Mononuclear Water Oxidation Catalyst Detected by *in Situ* X-ray Absorption Spectroscopy

- Dmitry Lebedev<sup>†</sup>
- Yuliana Pineda-Galvan<sup>‡</sup>
- Yuki Tokimaru<sup>§</sup>
- Alexey Fedorov<sup>†</sup>
- Nicolas Kaeffer<sup>†</sup>
- Christophe Copéret<sup>†\*</sup>
- Yulia Pushkar<sup>\*\*</sup>

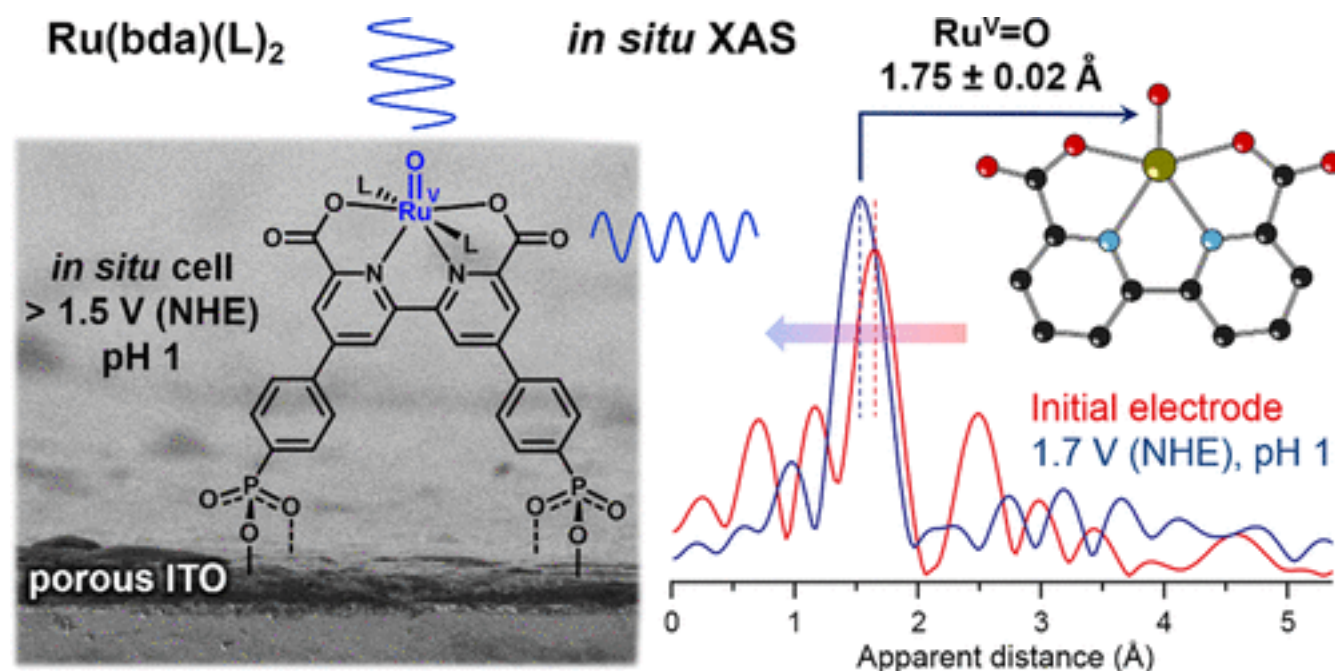
<sup>†</sup>ETH Zürich, Department of Chemistry and Applied Biosciences, Vladimir-Prelog-Weg 1-5, CH-8093 Zürich, Switzerland

<sup>‡</sup>Purdue University, Department of Physics and Astronomy, West Lafayette, Indiana 47907, United States

<sup>§</sup>Author Present Address :

Y.T.: The University of Tokyo, Graduate School of Engineering, Department of Chemistry and Biotechnology, 7-3-1 Hongo, Bunkyo-ku, 113-8656 Tokyo, Japan.

## Abstract



Improvement of the oxygen evolution reaction (OER) is a challenging step toward the development of sustainable energy technologies. Enhancing the OER rate and efficiency relies on understanding the water oxidation mechanism, which entails the characterization of the reaction intermediates. Very active Ru-bda type (bda is 2,2'-bipyridine-6,6'-dicarboxylate) molecular OER catalysts are proposed to operate via a transient 7-coordinate  $\text{Ru}^{\text{V}}=\text{O}$  intermediate, which so far has never been detected due to its high reactivity. Here we prepare and characterize a well-defined supported Ru(bda) catalyst on porous indium tin oxide (ITO) electrode. Site isolation of the catalyst molecules on the electrode surface allows trapping of the key 7-coordinate  $\text{Ru}^{\text{V}}=\text{O}$  intermediate at potentials above 1.34 V vs NHE at pH 1, which is characterized by electron paramagnetic resonance and *in situ* X-ray absorption spectroscopies. The *in situ* extended X-ray absorption fine structure analysis shows a  $\text{Ru}=\text{O}$  bond distance of  $1.75 \pm 0.02 \text{ \AA}$ , consistent with computational results. Electrochemical studies and density functional theory calculations suggest that the

water nucleophilic attack on the surface-bound  $\text{Ru}^{\text{V}}=\text{O}$  intermediate (O–O bond formation) is the rate limiting step for OER catalysis at low pH.

## Introduction

Hydrogen generated from renewable energy sources is an attractive sustainable fuel that does not contribute to global warming and  $\text{CO}_2$  emission in contrast to fossil fuels.(1) The most direct hydrogen production process is water splitting, which can be driven using either electrical (water electrolysis)(2) or solar (artificial photosynthesis) energy.(3) Water splitting is the sum of two half-reactions: hydrogen evolution reaction (HER, [eq 1](#)) at a cathode and oxygen evolution reaction (OER, [eq 2](#)) at an anode.  $2\text{H}^+ + 2\text{e}^- \rightarrow \text{H}_2$   
 (1)  $2\text{H}_2\text{O} \rightarrow \text{O}_2 + 4\text{H}^+ + 4\text{e}^-$  (2)

Whereas HER efficiently proceeds with low kinetic limitations (i.e., at low overpotentials) on noble metal catalysts such as Pt, OER shows sluggish kinetics, which currently limits the efficiency of the overall water splitting process.(4) The limitations originate from the complex multistep OER mechanism, which involves the transfer of four electrons and four protons transforming two water molecules into one oxygen molecule ([eq 2](#)). The improvement of water oxidation catalysts therefore requires understanding the detailed reaction mechanism and entails the characterization of reaction intermediates.(5)

The natural oxygen-evolving complex of the photosystem II consists of a  $[\text{Mn}_4\text{CaO}_5]$  cluster, which produces oxygen at rates of  $100\text{--}400\text{ s}^{-1}$ .(6) With the goal of mimicking activity of this very efficient cluster, artificial molecular catalysts based on coordination complexes of transition metals (Fe, Co, Ni, Cu, Mn, Ru, Ir)(7) have been developed and shown to be active in OER. Iridium(8) and ruthenium(9) complexes, in particular ruthenium complexes with a 2,2'-bipyridine-6,6'-dicarboxylate (bda) ligand,  $\text{Ru}^{\text{II}}(\text{bda})(\text{L})_2$  ([Figure 1a](#)), are among the most active OER catalysts in solution and therefore have attracted significant attention in the last 5 years.(10) The strongly electron-donating dianionic bda ligand bears two carboxylate groups, which can facilitate the formation of highly oxidized catalytic intermediates.(11)

**Figure 1**

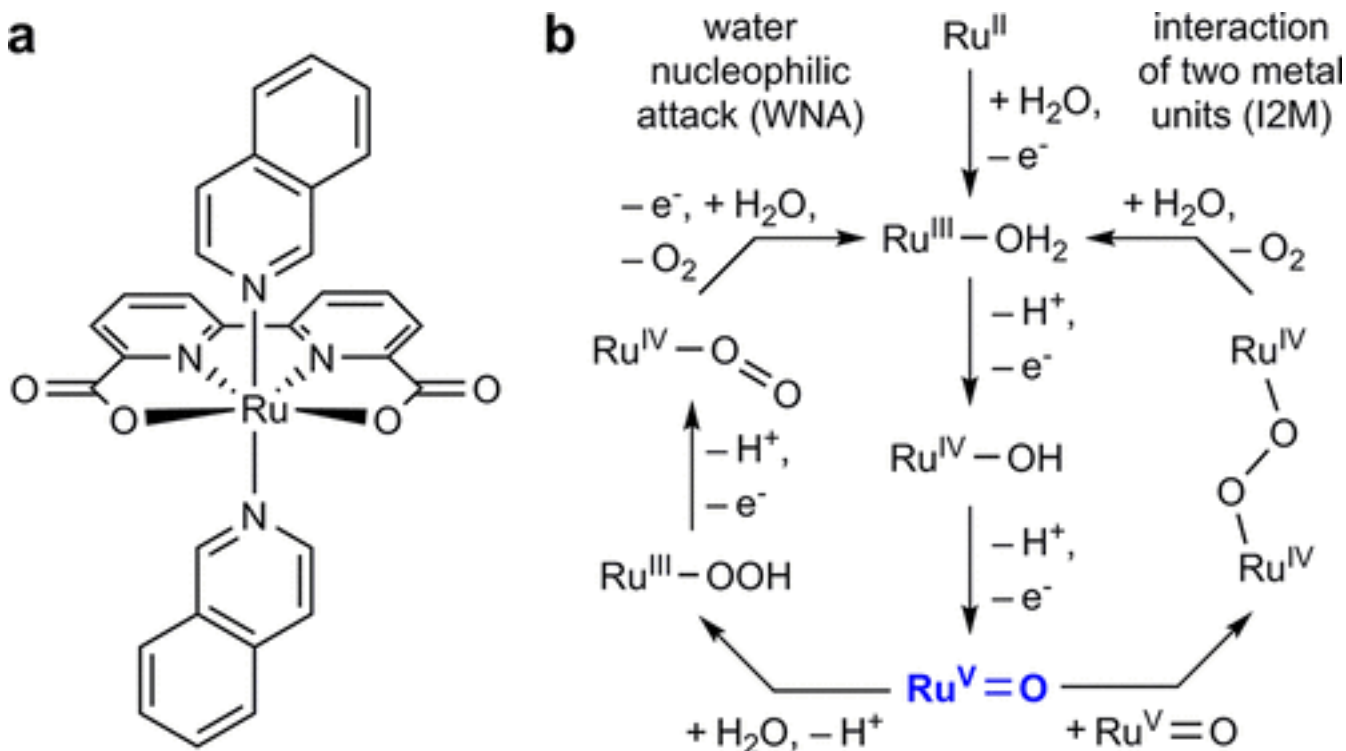


Figure 1. Structure of the [Ru(bda)(isoq)<sub>2</sub>] complex(10a) (a) and possible pathways of water oxidation for Ru-bda type complexes: I2M pathway is proposed to be predominant in solution, whereas WNA is expected for immobilized catalysts (b).

Molecular OER catalysts are proposed to function via two main types of mechanisms, which differ by the nature of the O–O bond formation step:(9, 12) a bimolecular mechanism involving the radical coupling of two metal oxo units (I2M) and a monomolecular mechanism involving the water nucleophilic attack (WNA) on a metal oxo species (Figure 1b). In both cases, the low-valent Ru intermediates are first oxidized through proton coupled electron transfer (PCET) steps to high-valent Ru<sup>IV</sup> or Ru<sup>V</sup> species. Both pathways share a common Ru<sup>V</sup>=O intermediate, which is responsible for the O–O bond formation and the overall reactivity. This key [Ru<sup>V</sup>=O(bda)(L)<sub>2</sub>]<sup>+</sup>intermediate has remained elusive and has never been detected and characterized experimentally.

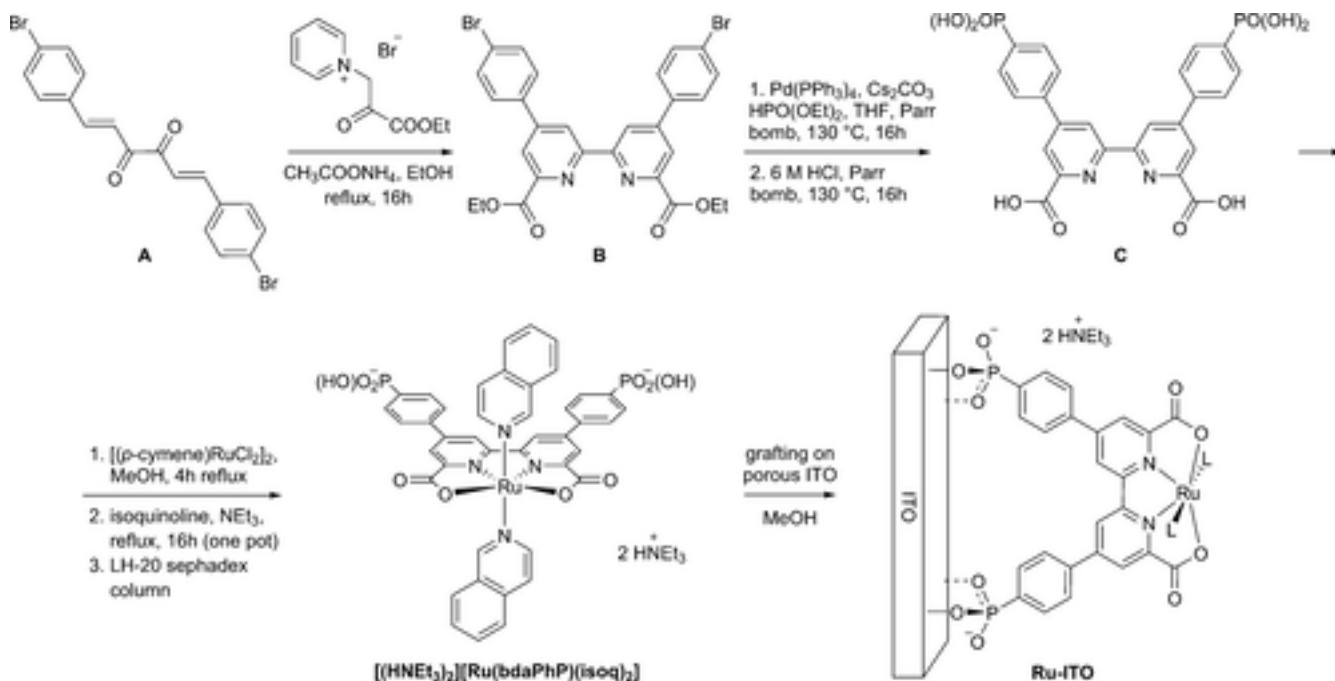
In fact, the direct spectroscopic observation and structural analysis of high-valent ruthenium species still remains a grand challenge. Currently, X-ray absorption (XAS) and electron paramagnetic resonance (EPR) spectroscopies have been used to characterize Ru<sup>V</sup>=O intermediates for [(bpy)<sub>2</sub>Ru<sup>II</sup>(H<sub>2</sub>O)<sub>2</sub>]<sup>2+</sup>(13) and [(bpy)<sub>2</sub>(H<sub>2</sub>O)Ru<sup>III</sup>ORu<sup>III</sup>(OH)<sub>2</sub>(bpy)<sub>2</sub>]<sup>4+</sup> (“blue dimer”; bpy, 2,2-bipyridine).(14) Both catalysts operate via PCET steps to access Ru<sup>V</sup>=O, which decreases the Ru<sup>V</sup>/Ru<sup>IV</sup> oxidation potential. On the other hand, for the [Ru<sup>II</sup>(bpy)(tpy)(H<sub>2</sub>O)]<sup>2+</sup> (tpy, 2,2';6',2''-terpyridine) catalyst,(15) EPR and XAS studies(16) could only detect the formation of [Ru<sup>IV</sup>(bpy)(tpy)=O]<sup>2+</sup>, while its oxidation to [Ru<sup>V</sup>(bpy)(tpy)=O]<sup>3+</sup> has never been observed experimentally. The lack of evidence for [Ru<sup>V</sup>(bpy)(tpy)=O]<sup>3+</sup> has been associated with the absence of PCET (no concomitant proton transfer), which therefore results in a high oxidation potential (computed to be 2.13 V vs RHE).(16a) A similar finding was obtained for the [Ru<sup>II</sup>(NPM)(4-pic)<sub>2</sub>(H<sub>2</sub>O)]<sup>2+</sup> (NPM, 4-*t*-butyl-2,6-di(1',8'-naphthyrid-2'-yl)-pyridine) catalyst.(17) Thereby, the formation of Ru<sup>V</sup>=O at modest oxidation potentials requires the Ru<sup>V</sup>/Ru<sup>IV</sup> transition to be a PCET step. Single-site Ru catalysts with neutral polypyridine ligands stabilize the Ru<sup>IV</sup>=O intermediate and possess high oxidation potential to Ru<sup>V</sup>=O due to the absence of concomitant proton transfer.(18)

For the Ru-bda type catalysts, it has long been hypothesized and indirectly confirmed by XRD (structure of the Ru<sup>IV</sup>–OH intermediate)(11) that the Ru center can adapt to a 7-coordinate geometry via binding a water molecule (OCO–Ru–OCO bond angle of 120–130°).(19) The 7-coordinate geometry and the anionic character of the bda ligand stabilize the Ru<sup>IV</sup> state as 7-coordinate hydroxo species [Ru<sup>IV</sup>–OH(bda)(L)<sub>2</sub>]. This is in contrast to the [Ru<sup>II</sup>(bpy)(tpy)(H<sub>2</sub>O)]<sup>2+</sup> catalyst and other 6-coordinate mononuclear analogues, which form Ru<sup>IV</sup>=O intermediates. Hence, the nature of the bda ligand makes the transition from Ru<sup>IV</sup> to Ru<sup>V</sup> a PCET (Figure 1b), which significantly lowers the corresponding oxidation potential to reach the postulated [Ru<sup>V</sup>=O(bda)(L)<sub>2</sub>]<sup>+</sup>species, making possible its experimental detection and characterization.

In solution [Ru<sup>V</sup>=O(bda)(L)<sub>2</sub>]<sup>+</sup> intermediates rapidly dimerize to form the O–O bond (I2M mechanism), which translates to high activity of the Ru-bda type catalysts.(10a) Conversely, upon immobilization on the electrode surface, the activity of the catalyst decreases, which has been associated with a change from the highly efficient I2M pathway in solution to the less efficient WNA pathway on the surface (Figure 1b).(20) We thus rationalize that generating well-defined surface-bound Ru(bda) species should provide a unique opportunity to ultimately trap the 7-coordinate [Ru<sup>V</sup>=O(bda)(L)<sub>2</sub>]<sup>+</sup> through site isolation, while enabling coupling of electrochemical measurements to advanced spectroscopic techniques.(21) Previous immobilization strategies have relied on anchoring Ru complexes via axial ligands,(20, 22) which was further exploited for integration of Ru-bda type catalysts in tandem devices.(23) However, the ease of dissociation of the axial ligand leads to catalyst degradation and loss of the device performance.(10b, 24)

Here, we thus develop a molecular Ru-complex that incorporates phosphonate anchoring groups(25) in the polydentate bda ligand, [(HNET<sub>3</sub>)<sub>2</sub>][Ru(bdaPhP)(isoq)<sub>2</sub>] (bdaPhP, 4,4'-bis(4-phosphonophenyl)-[2,2'-bipyridine]-6,6'-dicarboxylate) (Scheme 1), and graft the complex onto indium–tin oxide (ITO) electrodes. The use of the phosphonate anchoring groups in the polydentate bda ligand provides a sustained binding onto ITO electrodes and allows performance of extensive electrochemical and spectroscopic studies. Ultimately, using electron paramagnetic resonance (EPR) spectroscopy and *in situ* XAS, we detect and characterize the key high-valent 7-coordinate Ru<sup>V</sup>=O intermediate. The Ru=O distance of 1.75 Å measured by *in situ* extended X-ray absorption fine structure (EXAFS) spectroscopy is consistent with our computational findings.

## Scheme 1



Scheme 1. General Scheme of  $[(\text{HNEt}_3)_2][\text{Ru}(\text{bdaPhP})(\text{isoq})_2]$  Synthesis and Grafting

## Results and Discussion

### Synthesis, Immobilization, and Electrochemical Studies

$[(\text{HNEt}_3)_2][\text{Ru}(\text{bdaPhP})(\text{isoq})_2]$  complex was synthesized in a 5-step procedure (Scheme 1) starting from a condensation of two 4-bromobenzaldehyde molecules with diacetyl (detailed procedures are given in the Supporting Information). The obtained chalcone (**A**) was used to form bipyridine heterocycle (**B**) via Kröhnke method.<sup>(26)</sup> Next, the bromo moieties of the 4-bromophenyl substituent were converted into phosphonate groups using a Pd-catalyzed cross-coupling; a subsequent acid-catalyzed deprotection of both phosphonate and carboxylate groups provides the corresponding acid (**C**). The final complex was obtained by refluxing **C** with  $[(p\text{-cymene})\text{RuCl}_2]_2$  and isoquinoline followed by purification on Sephadex LH-20.  $[(\text{HNEt}_3)_2][\text{Ru}(\text{bdaPhP})(\text{isoq})_2]$  is immobilized on an ITO surface by grafting from a methanol solution on porous ITO electrodes, prepared by doctor blade method.<sup>(27)</sup>

The immobilized Ru complex (Ru-ITO) was first characterized by electrochemical measurements in 0.1 M  $\text{HClO}_4$  (pH 1) and 0.1 M acetate buffer (pH 5,  $I_t = 0.5$  M with  $\text{NaClO}_4$ ). At pH 1, cyclic voltammetry (Figure 2 and Figures S16 and S17) and differential pulse voltammetry (Figures S18 and S19) studies show the presence of three redox waves at 0.72, 1.06, and 1.34 V vs NHE followed by a slight current increase at high anodic potentials associated with the water oxidation (Figure S20). The linear dependence of the peak current at 0.72 V vs NHE (forward scan) with the scan rate indicates that the redox event is associated with the electrode-bound species (Figure S21). We attribute the observed redox waves to  $\text{Ru}^{\text{III}}/\text{Ru}^{\text{II}}$ ,  $\text{Ru}^{\text{IV}}/\text{Ru}^{\text{III}}$ , and  $\text{Ru}^{\text{V}}/\text{Ru}^{\text{IV}}$  transitions of the immobilized Ru complex (0.72, 1.06, and 1.34 V vs NHE, respectively, see Table S1 for details), in a good agreement with the previous studies of the Ru-bda type complexes.<sup>(10b, 20, 28)</sup> By integrating the  $\text{Ru}^{\text{III}}/\text{Ru}^{\text{II}}$  oxidation wave, we estimated the loading of immobilized Ru complex as  $14 \pm 2$  nmol  $\text{cm}^{-2}$  for 2  $\mu\text{m}$  thick electrodes and  $100 \pm 15$  nmol  $\text{cm}^{-2}$  for thicker electrodes, which were used for stability and XAS studies. These values are comparable to the previously published loadings on porous ITO electrodes.<sup>(27)</sup>

## Figure 2



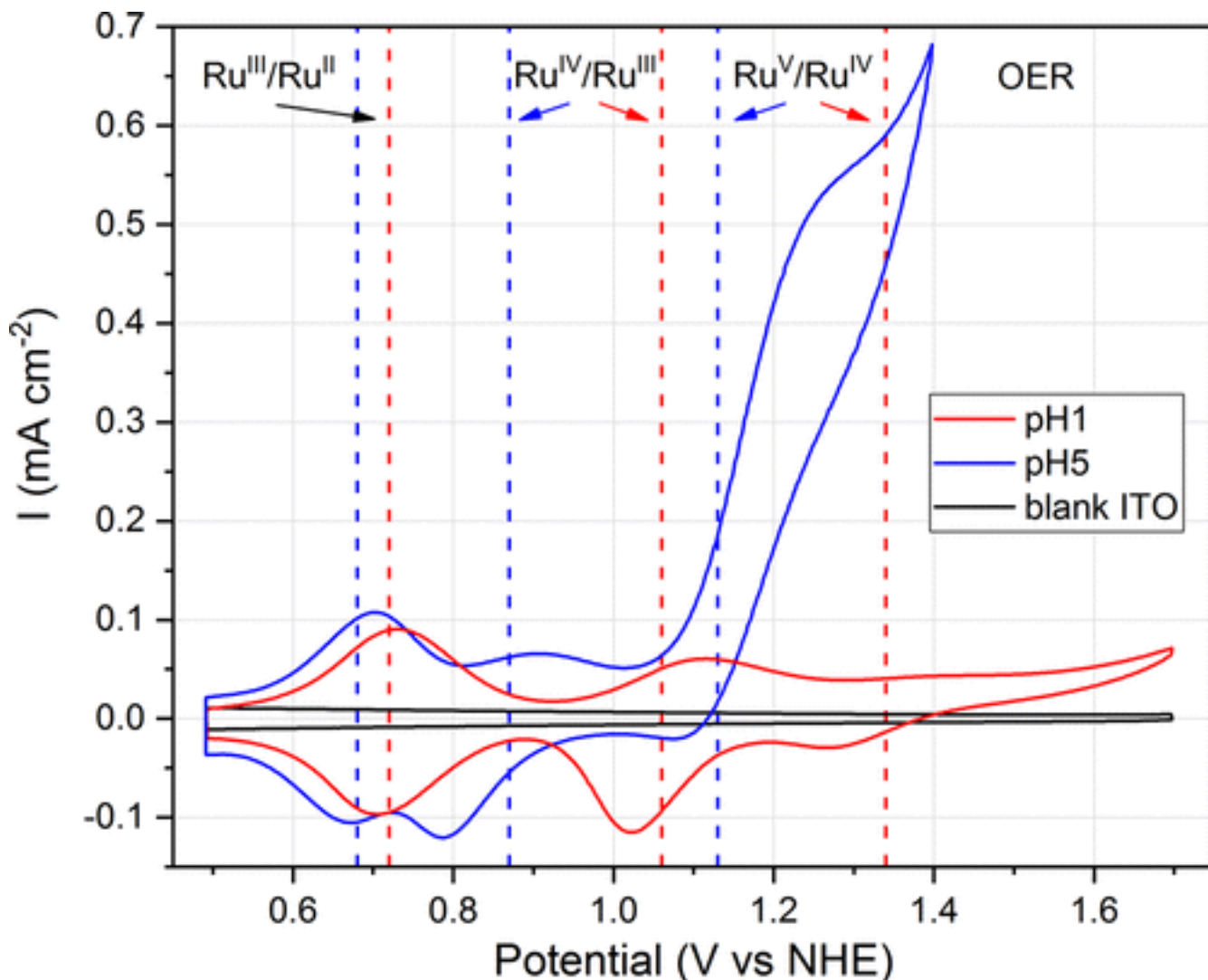


Figure 2. Cyclic voltammograms of ITO and Ru-ITO electrodes recorded at a scan rate of  $10 \text{ mV s}^{-1}$  in  $0.1 \text{ M HClO}_4$  (pH 1) and  $0.1 \text{ M}$  acetate buffer (pH 5,  $I_t = 0.5 \text{ M}$  with  $\text{NaClO}_4$ ).  $\text{Ru}^{\text{III}}/\text{Ru}^{\text{II}}$  couple does not show significant pH dependence, whereas  $\text{Ru}^{\text{IV}}/\text{Ru}^{\text{III}}$  and  $\text{Ru}^{\text{V}}/\text{Ru}^{\text{IV}}$  couples shift with pH change, consistent with PCET processes.

At pH 5,  $\text{Ru}^{\text{III}}/\text{Ru}^{\text{II}}$  and  $\text{Ru}^{\text{IV}}/\text{Ru}^{\text{III}}$  redox waves are also observed, while the  $\text{Ru}^{\text{V}}/\text{Ru}^{\text{IV}}$  event ( $1.13 \text{ V}$  vs NHE) superimposes with the current increase, associated with OER catalysis (Figure 2). As seen by higher OER currents at pH 5 compared to pH 1 (Figure S20), the immobilized complex is more active in near neutral conditions, consistent with the literature reports.(28)

Using perchloric acid, phosphate, and acetate buffer solutions, we studied the pH dependence of the redox couples in the pH range from 0 to 8, which allowed us to construct the Pourbaix ( $E_{1/2}$  vs pH) diagram of Ru-ITO (Figure S22). In pH range from 0 to 6, the Pourbaix diagram shows that the  $\text{Ru}^{\text{III}}/\text{Ru}^{\text{II}}$  redox couple is pH independent, while  $\text{Ru}^{\text{IV}}/\text{Ru}^{\text{III}}$  and  $\text{Ru}^{\text{V}}/\text{Ru}^{\text{IV}}$  redox transitions are proton-coupled electron transfers, consistent with the mechanism shown in Figure 1b.(20, 28) In addition, the data obtained from UV-visible spectroelectrochemistry (Figures S23 and 24) corroborates well the assignment and agrees with previous studies on Ru-bda type complexes.(20, 29)

To assess the stability of the immobilized complex, we contacted Ru-ITO electrode with pH 1 electrolyte for 1 h and analyzed the solution by  $^1\text{H}$  NMR spectroscopy. We found no signature of  $[\text{Ru}(\text{bdaPhP})(\text{isoq})_2]$  detachment; however we observe the release of isoquinoline (Figures S25–27) into solution. This observation points at the lability of the axial ligand and validates our anchoring strategy via the bda backbone. After 2 h of electrolysis at  $1.5 \text{ V}$  vs NHE, cyclic voltammetry demonstrated that ca. 30% of the initial complex was still electroactive, but  $^1\text{H}$  and  $^{31}\text{P}$  NMR of the liquid phase detect no possible degradation products of the bda ligand (Figures S26 and 27). We postulate that the loss of the electroactive centers might originate from partial degradation of the complex into a broad range of species (which are below the NMR limit of detection) or blocking of the ITO pores by oxygen bubbles, which makes the Ru centers inaccessible to electrolyte.

In order to observe transient Ru species, the Ru-ITO electrodes were investigated by *ex situ* X-band electron paramagnetic resonance (EPR) spectroscopy. The Ru-ITO electrodes were polarized (pH 1) to a given potential and then quickly taken out of the electrolyte solution and immediately frozen in liquid nitrogen (see the [Supporting Information](#) for more experimental details). At 0.9 V vs NHE, the EPR spectrum indicates the formation of Ru<sup>III</sup> species ([Figure S28](#));(19) increasing the potential to 1.7 V vs NHE ([Figure S28](#)) generates Ru<sup>V</sup> species,(13, 30) as indicated by two components at  $g_{xx} = 2.07$  and  $g_{yy} = 2.00$ . The  $g_{zz}$  component, reported at  $g_{zz} = 1.85$ – $1.91$ ,(13, 30) is likely obscured by the background signal of the ITO. The Ru<sup>V</sup> EPR signal is short-lived and disappears upon sample melting ([Figure S29](#)). The Ru<sup>IV</sup> state is EPR silent and therefore cannot be detected. Since the limitations of EPR do not allow for full characterization of the reaction intermediates, we turn to more detailed investigation of the Ru-ITO system using *in situ* XAS.

### ***In Situ* Characterization of the Immobilized Catalysts by XAS**

To reliably investigate the oxidation state of the Ru center and probe the Ru coordination environment, we exploited *in situ* XAS studies of the immobilized complex at Ru K-edge ([Figure 3](#)). First, the Ru-ITO electrode is studied outside of the electrochemical cell (initial electrode, see [Figures S30–32](#)). Multiple XAS scans yield consistent spectra without change in Ru K-edge spectrum or the brown color of the electrode, indicating no X-ray induced damage of the immobilized ruthenium complex. Partial oxidation of the initial electrode by atmospheric oxygen (admixture of the Ru<sup>III</sup> state) leads to the slight shift of the edge position toward higher energies as compared to the pure Ru<sup>II</sup> state obtained *in situ* electrochemically ([Figure S31](#), *vide infra*).

## **Figure 3**

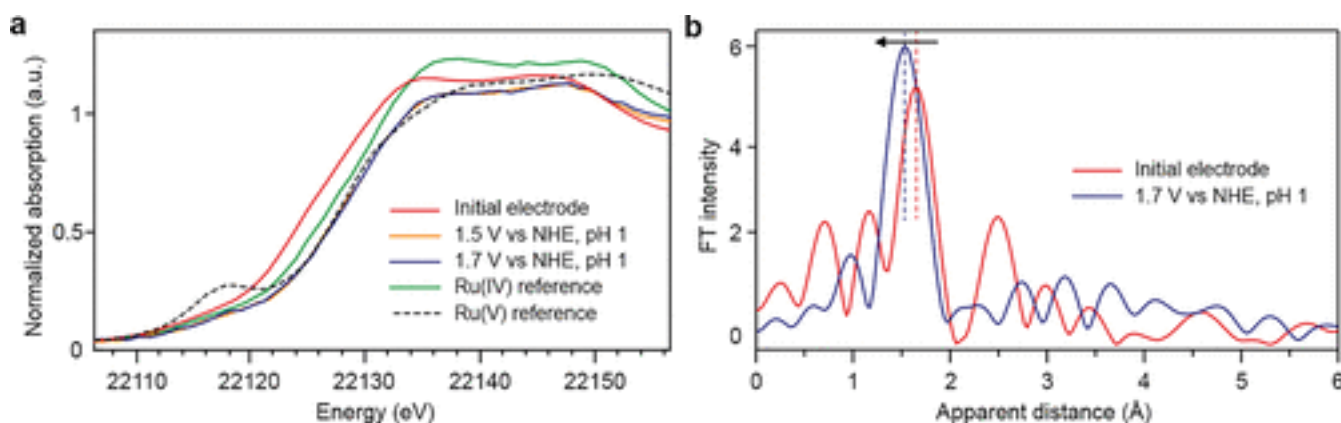


Figure 3. *In situ* XAS of Ru-ITO electrodes. Ru K-edge XANES of the initial electrode outside of the cell and *in situ* XANES of Ru-ITO in 0.1 M HClO<sub>4</sub> at 1.5 and 1.7 V vs NHE, indicating formation of Ru<sup>V</sup> species (reference compounds are Ru<sup>IV</sup>O<sub>2</sub> and [(<sup>n</sup>Pr<sub>4</sub>N)][Ru<sup>V</sup>(O)(2-hydroxy-2-ethylbutyrato)<sub>2</sub>]) (a). Fourier transforms of  $k^3$ -weighted Ru EXAFS spectra (3.86–11.83  $k$ -space) of the initial electrode measured outside of the electrochemical cell (red) and *in situ* at pH 1 at potential above 1.5 V vs NHE (blue) (b). The shift of the maximum of the peak corresponding to the first coordination sphere indicates contribution of the short Ru<sup>V</sup>=O backscatter at  $1.75 \pm 0.02$  Å.

The Fourier transform of the EXAFS spectrum of Ru-ITO ([Figure 3b](#)) shows scattering events corresponding to the first and second coordination shells of ruthenium. We have fitted the EXAFS data (see [Table 1](#), [Figures S33 and S34](#) and [Supporting Information](#) for fitting details) using the model derived from [Ru(bda)(isoq)<sub>2</sub>] structure (Density Functional Theory calculations, *vide infra*). In [Ru(bda)(isoq)<sub>2</sub>], ruthenium is surrounded by the disordered shell of four nitrogen atoms and two oxygen atoms. Sufficiently good EXAFS fits are obtained using six identical neighbors (nitrogen) in the first shell and ten carbon atoms in the second shell ([Table 1](#)). Overall, the resulting Ru–N distance of  $2.09 \pm 0.02$  Å is in a good agreement with the average Ru–O/N distance of the first coordination shell (2.07 Å for [Ru(bda)(4-picoline)<sub>2</sub>] at room temperature).(11) Splitting the first coordination shell into four nitrogen and two oxygen atoms in accordance with the chemical structure results in the same quality fits ([Figure S35](#)). Relatively high Debye–Waller parameters show that the first coordination shell is indeed disordered, and thus the exact determination of the number of nitrogen and oxygen backscatterers at  $\sim 2.1$  Å purely from EXAFS is not possible.

### **Table 1. EXAFS Fits for Ru-ITO Electrodes<sup>a</sup>**

fit	shell, $N_b$	$R$ , Å	$\sigma^2 \times 10^3$ , Å <sup>2</sup>	$R$ -factor	reduced $\chi^2$
<b>Initial Electrode (outside of the electrochemical cell)</b>					
<b>3.86–13.3 <math>k</math>-space, 1.32–3.12 <math>R</math>-space</b>					
1	Ru–N, 6	2.09	9.0	0.112	11123
2	Ru–N, 6	2.09	7.9	0.027	3691
	Ru–C, 10	2.97	12.1		
3	Ru–N, 6	2.09	8.0	0.0097	1591
	Ru–C, 8	2.97	7.4 <sub>c</sub>		
	Ru–C, 2	3.19	7.4		
<b>Electrode at the Oxidizing Potential above 1.5 V vs NHE</b>					
<b>3.86–11.83 <math>k</math>-space, 1.1–3.12 <math>R</math>-space</b>					
4	Ru–N, 6	2.06	6.4	0.0733	5212
5	Ru–N, 6	2.04	5.5	0.0308	3062
	Ru–C, 10	2.95	16.4		
6	Ru–O, 1	1.75	1.0	0.0009	109
	Ru–N, 6	2.13	9.8		
	Ru–C, 10	3.13	21.0		
<b>Electrode at the Oxidizing Potential above 1.5 V vs NHE</b>					
<b>3.86–10.7 <math>k</math>-space, 1.19–2.1 <math>R</math>-space</b>					
7	Ru–N, 6	2.09	6.7	0.0150	4313
8	Ru–O, 1	1.75	2.0	0.0003	591
	Ru–N, 6	2.12	8.5		

<sup>a</sup>

$N$ , coordination number;  $R$ , distance between absorber and backscatter atoms;  $\sigma^2$ , the Debye–Waller factor. Amplitude reduction factor  $S_0^2$  was set to 1. Errors were estimated as  $R - \pm 1\%$ ;  $\sigma^2 - \pm 20\%$ .

<sup>b</sup>

First shell was modeled as six nitrogen atoms, as splitting the shell did not statistically improve the fit (see text for the discussion).



The same parameter was used for multiple shells.

We further proceeded with *in situ* X-ray absorption near edge spectroscopy (XANES) in order to follow the evolution of the absorption edge as a function of applied potential and characterize the postulated Ru<sup>V</sup>=O intermediate. *In situ* data are collected in a custom cell (see [Supporting Information](#) for details) in 0.1 M HClO<sub>4</sub> (pH 1) and 0.1 M acetate buffer (pH 5, I<sub>t</sub> = 0.5 M with NaClO<sub>4</sub>).

At pH 1, we observe a gradual increase of the edge energy with increase of the applied potential ([Figure 3a](#) and [Figures S30 and S32](#)), which we assign to transitions from Ru<sup>II</sup> (0–0.4 V vs NHE) to Ru<sup>III</sup> (0.9 V vs NHE) and further to Ru<sup>IV</sup> (1.25 V vs NHE) and Ru<sup>V</sup> (1.5–1.7 V vs NHE) states. The highest Ru K-edge energy is achieved at 1.5 V vs NHE and increase of the applied potential to 1.7 V vs NHE does not change the Ru K-edge position, indicating no further oxidation ([Figure 3a](#)). Comparison of these spectra with the spectra of two reference compounds, Ru<sup>IV</sup>O<sub>2</sub> and [(<sup>n</sup>Pr<sub>4</sub>N)][Ru<sup>V</sup>(O)(2-hydroxy-2-ethylbutyrate)<sub>2</sub>],(31) shows that the oxidation state is above +4 and close to +5 ([Figure 3a](#)).

We note that the intensity of the XANES pre-edge feature is significantly lower in the case of Ru-ITO as compared to the reference Ru<sup>V</sup> compound. Intensity of the pre-edge feature is determined by the mixing of the O 2p orbitals with Ru 4d orbitals, which makes otherwise dipole forbidden transition from Ru 1s to 4d level partially allowed. Shorter Ru=O bond length results in a larger degree of oxygen orbital mixing and therefore higher intensity of the pre-edge feature.(16b, 32) We have performed population analysis of the three Ru complexes using Density Functional Theory (DFT) calculations (see details in the Supporting Information, [Figure S39](#) and [Table S2](#)): the reference Ru<sup>V</sup>=O compound, [Ru<sup>V</sup>=O(bda)(isoq)<sub>2</sub>]<sup>+</sup>, and [Ru<sup>IV</sup>=O(tpy)(bpy)]<sup>2+</sup>.(16a) We find much lower degree of O 2p – Ru 4d orbital mixing in [Ru<sup>V</sup>=O(bda)(isoq)<sub>2</sub>]<sup>+</sup> as compared to the reference Ru<sup>V</sup>=O compound, which transforms into lower intensity of the XANES pre-edge feature. Therefore, our XANES results point out that the Ru<sup>V</sup> state observed for the Ru-ITO should feature a longer Ru=O bond compared to ~1.70 Å for [(<sup>n</sup>Pr<sub>4</sub>N)][Ru<sup>V</sup>(O)(2-hydroxy-2-ethylbutyrate)<sub>2</sub>].

Recording *in situ* EXAFS of a molecular complex on the electrode surface is highly challenging because of the low content of molecular species and significant scattering of the X-rays by the supporting electrode materials and electrolyte. To the best of our knowledge, there are only few reports on *in situ* XAS studies of thin films(33) and none for immobilized molecular water oxidation catalysts. In an attempt to characterize the Ru<sup>V</sup>=O species via EXAFS, the electrode potential was held at 1.5 or 1.7 V vs NHE. As the immobilized Ru complex displays only minor catalytic activity at pH 1, the current quickly dropped to ~5 μA cm<sup>-2</sup> (1.5 V vs NHE) and remained constant throughout the measurement. We have recorded multiple XAS spectra at 1.5 and 1.7 V vs NHE ([Figure 3b](#)); consecutive scans show no changes in the absorption spectrum. Obtained data were fitted using the same model as described above for initial electrode with the addition of the short Ru=O backscatterer ([Table 1](#), see the Supporting Information and [Figures S36–38](#) for more details). We found that the addition of the short Ru=O backscatterer to the first coordination shell is vital to achieve a good fit of the EXAFS data (Fits 6 and 8 in [Table 1](#)). Additional splitting of the first coordination shell into four nitrogen and two oxygen atoms in accordance with the chemical structure yielded the same quality fits similar to the results obtained for the initial electrode ([Figure S38](#)). Multiple electrodes used during two beam times consistently yielded similar results. We obtain a Ru=O bond distance of 1.75 ± 0.02 Å. This distance is longer than the one reported for the “blue dimer” Ru<sup>IV</sup>,Ru<sup>V</sup> intermediate (~1.70 Å)(14b, 14c) and the reference Ru<sup>V</sup> complex (1.70 Å),(31) in line with the much lower intensity of the pre-edge XANES feature for Ru-ITO as compared to Ru<sup>V</sup> reference. However, the distance is shorter than ~1.80 Å reported for Ru<sup>IV</sup>=O complexes.(14c, 16a) We also note that the obtained distance agrees with the results of the computational study (*vide infra*). For comparison, X-ray crystal structure data of the 7-coordinate [Os<sup>V</sup>=O(qpy)(4-picoline)(Cl)]<sup>2+</sup> (qpy, 2,2':6',2'':6'':2'''-quaterpyridine) revealed the Os=O distance of 1.74 Å.(34) Finally, in order to verify our fitting approach, we tried adding the short Ru=O backscatterer to the EXAFS model of the initial electrode and found that this does not improve the fit (results in an increase of χ<sup>2</sup>).

To test for the formation of RuO<sub>2</sub> from decomposition of the Ru catalyst, as recently reported on a similar system,(22b) we polarized the electrode back to 0.1 V vs NHE after the EXAFS measurement (1.5 h at 1.7 V vs NHE). We observed a color change back to brown (signature of the Ru<sup>II</sup> state) and the recovery of the Ru K-edge position characteristic of Ru<sup>II</sup> ([Figure S31](#)). Therefore, we rule out the degradation of the grafted Ru complex into RuO<sub>2</sub> under our experimental conditions.

XANES studies of the immobilized complex at pH 5 (Figure S32) show that at 1.3 and 1.5 V vs NHE the Ru oxidation state is close to +4 (reference RuO<sub>2</sub>). This observation indicates that the Ru<sup>V</sup>=O intermediate could not be observed at higher pH since it is more reactive toward water, as supported by larger catalytic current at pH 5 compared to pH 1 (Figure 2 and Figure S20).

## DFT Studies and Discussion of the Mechanism

To evaluate the possible reaction pathway and likely reaction intermediates, we performed DFT calculations using the model with five explicit water molecules(19) and a simplified bda ligand without phenyl substituents (see more details of the DFT calculations in Supporting Information). The energies of different intermediate states are given in Table S3 and the proposed mechanistic pathway is shown as a dotted line on the Latimer–Frost diagram in Figure 4. Based on our calculation results and earlier literature reports,(28)we hypothesize that, at pH 1, the Ru<sup>II</sup> complex undergoes protonation and decoordination of one carboxylate ligand with coordination of one water molecule to the Ru center (a to b, carboxylate-off 6-coordinate Ru). The next step is a pH independent one-electron oxidation of Ru<sup>II</sup> to Ru<sup>III</sup> without a change of the geometry (b to c, non PCET, in agreement with experimental data, Figure S22) followed by deprotonation and coordination of the carboxylate transition to the 7-coordinate Ru (d), in line with recently published EPR study.(19) The subsequent oxidation steps from Ru<sup>III</sup> to Ru<sup>IV</sup> (d to e) and Ru<sup>IV</sup> to Ru<sup>V</sup> (e to f) correspond to PCET steps. Calculated redox potentials are found to be in good agreement with the experimental values, supporting the formation of Ru<sup>V</sup> state in the form of Ru<sup>V</sup>=O intermediate (Table S1).

Figure 4

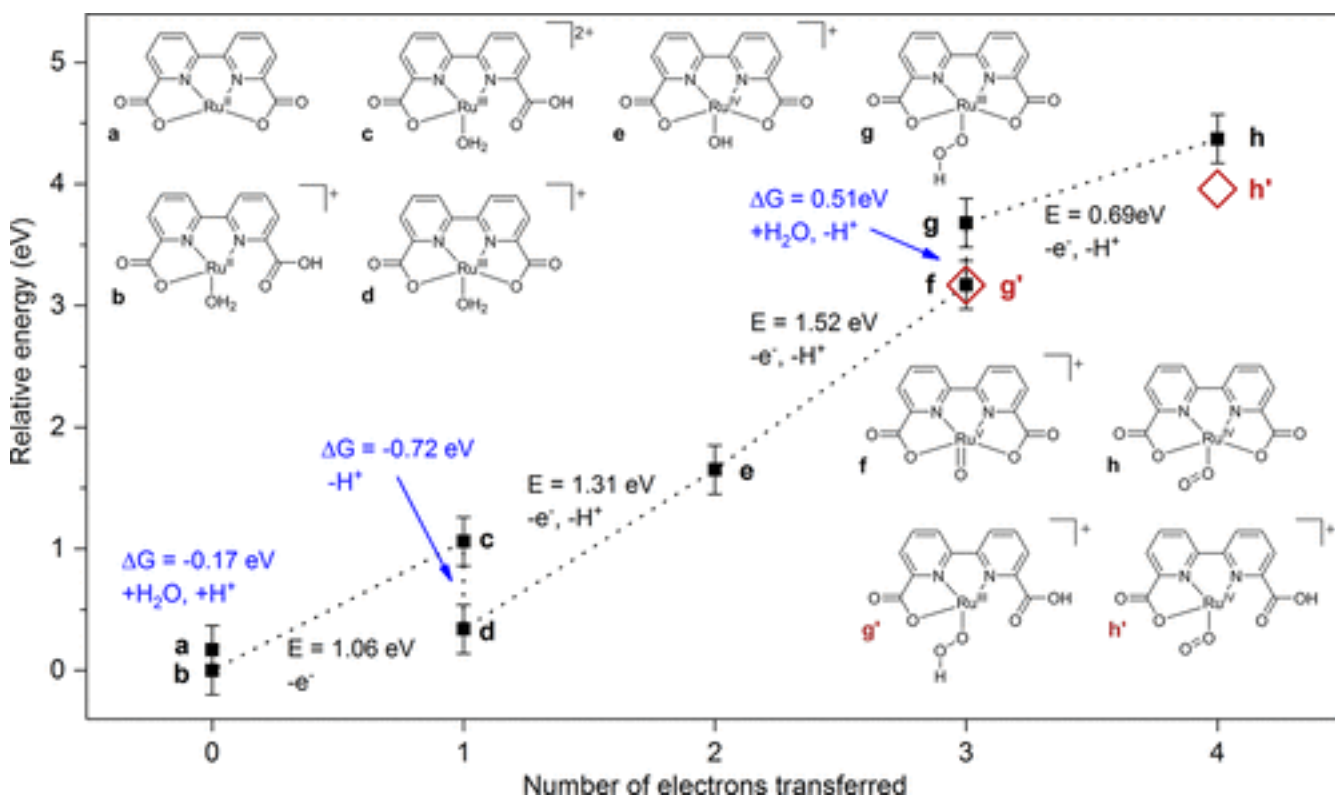


Figure 4. Calculated Latimer–Frost diagram for the proposed WNA mechanism. Dotted line indicates the proposed oxidation pathway. Energies of chemical and electrochemical transitions are shown as  $\Delta G$  and  $E$  in blue and black, respectively. Seven-coordinate Ru<sup>V</sup>=O intermediate is shown as f, red diamonds g' and h' correspond to the pathway with COO-assisted WNA step (see text for the discussion).

Our calculations show that the 7-coordinate [Ru<sup>V</sup>=O(bda)(isoq)<sub>2</sub>]<sup>+</sup>intermediate (f and Figure 5) is the most stable form of Ru<sup>V</sup>. Its conversion to the 6-coordinate complex (carboxylate-off) has a  $\Delta G$  of +0.7 eV, while a  $\Delta G$  of +0.3 eV (pH 1) is found for the 6-coordinate complex with protonated COOH group (Table S4). We find that during the DFT energy minimization the latter six-coordinate complex can convert to the 7-coordinate [Ru<sup>V</sup>=O(bda-COOH)(isoq)<sub>2</sub>], which is ~0.2 eV higher in energy than the unprotonated complex, indicating that the 7-coordinate geometry is strongly preferred for the high-valent Ru intermediates.

Figure 5

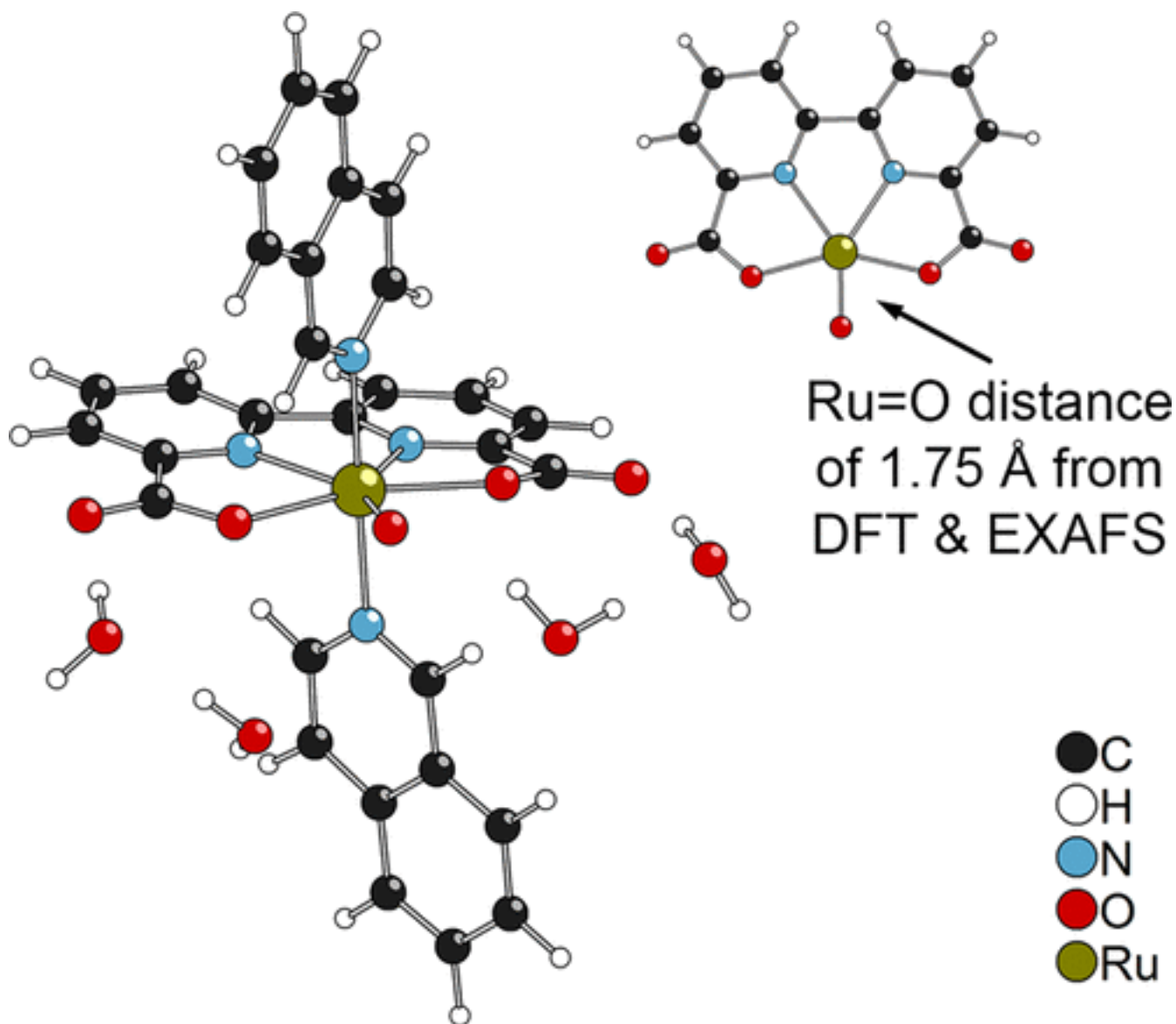


Figure 5. DFT optimized structure of the  $[\text{Ru}^{\text{V}}=\text{O}(\text{bda})(\text{isoq})_2]^+$  intermediate with four explicit water molecules; inset, the equatorial plane with tetradentate bda ligand and the key  $1.75 \pm 0.02 \text{ \AA}$   $\text{Ru}^{\text{V}}=\text{O}$  bond (isoquinoline ligands are omitted for clarity).

The DFT level of theory used here was previously shown to reproduce  $\text{Ru}-\text{X}$  bond distances within the experimental precision of the EXAFS distance analysis ( $\pm 0.02 \text{ \AA}$ ).<sup>(16)</sup> The calculated  $\text{Ru}=\text{O}$  distance in the 7-coordinate  $[\text{Ru}^{\text{V}}=\text{O}(\text{bda})(\text{isoq})_2]^+$  state (**f**) is found to be  $1.75 \text{ \AA}$ , which matches very well with the experimental value obtained from EXAFS ( $1.75 \pm 0.02 \text{ \AA}$ ). For the 6-coordinate complex, we calculated a shorter  $\text{Ru}=\text{O}$  distance of  $1.72 \text{ \AA}$  (Table S3). The 7-coordinate  $[\text{Ru}^{\text{V}}=\text{O}(\text{bda})(\text{isoq})_2]^+$  (**f**) shows all the features of the potentially reactive species with radicaloid character of the  $\text{Ru}^{\text{V}}=\text{O}$  oxygen with the spin density  $\rho_0 = 0.7$  (Figure S40). In solution, this highly reactive species would quickly engage in a bimolecular radical coupling process (I2M pathway, Figure 1b). For the Ru-ITO electrodes, the I2M pathway is very unlikely because of the site isolation provided by surface-immobilization of  $[\text{Ru}(\text{bdaPhP})(\text{isoq})_2]$  species,<sup>(22a, 28, 29)</sup> which makes the WNA mechanism more probable for our system and therefore allows for detection and characterization of the  $\text{Ru}^{\text{V}}=\text{O}$  intermediate.

In the WNA mechanism, the nucleophilic attack of a water molecule on  $\text{Ru}^{\text{V}}=\text{O}$  is often considered as the rate determining step in the catalytic cycle.<sup>(28, 35)</sup> In acidic pH, we have found that this transition (**f** to **g**) is uphill in energy ( $0.5 \text{ eV}$  at pH 1), in line with low OER activity of the surface-attached complex. Increase of the pH (and presence of base) facilitates the O–O bond formation from  $\text{Ru}^{\text{V}}=\text{O}$  (**f**) to  $\text{Ru}^{\text{III}}-\text{OOH}$  (**g**)<sup>(22a, 28)</sup> and results in faster OER catalysis (Figure 2 and Figure S20). As a consequence,  $\text{Ru}^{\text{V}}=\text{O}$  is likely not the major resting state in more basic media. This argument is consistent with the lower XANES edge energy recorded under electrocatalytic turnover at pH 5 as compared to pH 1 (Figure S32), indicating a shift toward less oxidized Ru species. We also note a  $\Delta G \approx 0 \text{ eV}$  for the reaction of  $[\text{Ru}^{\text{V}}=\text{O}(\text{bda})(\text{isoq})_2]^+$  (**f**) with a water

molecule to form the protonated  $[\text{Ru}^{\text{III}}\text{-OOH}(\text{bda-COOH})(\text{isoq})_2]^+(\mathbf{g}')$  intermediate (red diamonds on [Figure 4](#)). While this value would indicate that the carboxylate ligand might act as an internal base facilitating WNA, low activity of the immobilized complex at acidic pH and the base-enhancement of catalysis(20, 28) do not support this hypothesis.(36)

Taken together, EPR data, combined evidence of the low XANES pre-edge intensity, the XANES edge energy, and the 1.75 Å Ru=O distance determined by EXAFS and DFT analyses have allowed us to characterize the elusive  $\text{Ru}^{\text{V}}=\text{O}$  7-coordinate intermediate. Its observation and detailed characterization is possible only because of the use of appropriate immobilization strategy and pH conditions (pH 1) under which this highly reactive intermediate has low reactivity toward O–O bond formation.

## Conclusions

We have designed and synthesized the  $[(\text{HNEt}_3)_2][\text{Ru}(\text{bdaPhP})(\text{isoq})_2]$  complex bearing two phosphonate binding groups on the polydentate bda ligand. The complex was successfully immobilized on the surface of porous ITO electrodes and characterized by electrochemical and *in situ* spectroscopic methods. We determined the  $\text{Ru}^{\text{V}}/\text{Ru}^{\text{IV}}$  redox potential to be 1.34 V vs NHE at pH 1 and observed that  $\text{Ru}^{\text{IV}}\text{-OH}$  to  $\text{Ru}^{\text{V}}=\text{O}$  oxidation is a PCET step, as expected from previous reports.(10b) We found that the subsequent water nucleophilic attack is a rate determining step at pH 1. This is supported by DFT calculations ( $\Delta G$  of +0.5 eV for  $\text{Ru}^{\text{V}}=\text{O} + \text{H}_2\text{O} \rightarrow \text{Ru}^{\text{III}}\text{-OOH}$  at pH 1) and electrochemical data, which reveal minor OER activity of the immobilized complex in acidic conditions and increase of the activity at higher pH (base-enhanced catalysis).(28) The high barrier for the WNA step in acidic environment and the use of advanced *in situ* XAS techniques allowed detecting and characterizing the key 7-coordinate  $\text{Ru}^{\text{V}}=\text{O}$  intermediate. The Ru=O distance was measured to be  $1.75 \pm 0.02$  Å, consistent with our DFT calculations.

Overall, *ex situ* EPR and *in situ* XAS data validate the central proposals for the mechanism and activity of one of the most efficient classes of molecular water oxidation catalysts based on Ru-bda unit. The detailed understanding of the reaction mechanism constitutes a key step toward the development of active and stable Ru-based OER catalysts. Stable catalysts that can access high-valent oxo states at low overpotentials and achieve fast O–O bond formation would be ideal candidates for electrode immobilization toward integration in overall water-splitting devices.

## Experimental Section

Detailed procedures for the synthesis, characterization, and immobilization of  $[(\text{HNEt}_3)_2][\text{Ru}(\text{bdaPhP})(\text{isoq})_2]$  are given in the [Supporting Information](#).

Electrochemical measurements were performed in a standard single-compartment 3-electrode cell using PGSTAT128N Autolab potentiostat. The porous ITO electrodes were electrically contacted using the uncoated FTO layer and masked to a geometrical surface area of 1.5 cm<sup>2</sup>. A piece of a platinum mesh served as the counter electrode and saturated Ag/AgCl electrode served as the reference electrode. Electrolytes were saturated with N<sub>2</sub> prior to the measurements. All reported measurements were repeated several times to ensure the reproducibility of results. Spectroelectrochemical studies were performed using Cary 5000 UV–vis–NIR spectrometer (1010 nm min<sup>-1</sup>, resolution of 1.1 nm) and PGSTAT101 Autolab potentiostat using the same conditions as used for electrochemical studies.

X-band EPR studies were performed at 20 K; details of the measurements can be found in the [Supporting Information](#).

*In situ* XAS studies were performed in a custom made electrochemical cell (20 mL) at the Advanced Photon Source (APS), Argonne National Laboratory at electron energy of 23 keV in the fluorescence mode. EXAFS data were analyzed using the Athena software package.(37)

Density functional theory (DFT) calculations were performed with Gaussian09 using the B3LYP exchange-correlation (XC) functional. The energy uncertainty is estimated to be 0.2 eV.

The full description of methods and procedures is given in the [Supporting Information](#).

## Supporting Information

The Supporting Information is available free of charge on the [ACS Publications website](#) at DOI: [10.1021/jacs.7b11388](https://doi.org/10.1021/jacs.7b11388).



- Synthesis, characterization, and immobilization of [(HNEt<sub>3</sub>)<sub>2</sub>][Ru(bdaPhP)(isoq)<sub>2</sub>] complex, additional experimental details and data (electrochemical, spectroelectrochemical, EPR, XAS), details of the DFT calculations, and energies and atomic coordinates of intermediates ([PDF](#))

The authors declare no competing financial interest.

## Acknowledgment

---

This research is based upon work supported by Swiss Competence Center for Energy Research (SCCER) Heat & Electricity Storage and the U.S. Department of Energy, Office of Basic Energy Sciences, under Award DE-FG02-10ER16184 (Y.P.). The use of the Advanced Photon Source, an Office of Science User Facility operated by the U.S. Department of Energy (DOE) Office of Science by Argonne National Laboratory, was supported by the U.S. DOE under Contract DE-AC02-06CH11357. The PNC/XSD (Sector 20) facilities at the Advanced Photon Source and research at these facilities were supported by the U.S. Department of Energy—Basic Energy Science and the Canadian Light Source. Y.T. is grateful to the Japan Society for the Promotion of Science (JSPS) for a Research Fellowship for Young Scientists.

## References

---

This article references 37 other publications.

1. **1**

---

Turner, J. A. *Science* **2004**, 305, 972DOI: 10.1126/science.1103197

[\[Crossref\]](#), [\[PubMed\]](#), [\[CAS\]](#), [Google Scholar](#) [open URL](#)

---

2. **2**

---

Ursua, A.; Gandia, L. M.; Sanchis, P. *Proc. IEEE* **2012**, 100, 410DOI: 10.1109/JPROC.2011.2156750

[\[Crossref\]](#), [\[CAS\]](#), [Google Scholar](#) [open URL](#)

---

3. **3**

---

(a) Kim, D.; Sakimoto, K. K.; Hong, D.; Yang, P. *Angew. Chem., Int. Ed.* **2015**, 54, 3259DOI: 10.1002/anie.201409116

[\[Crossref\]](#), [\[PubMed\]](#), [\[CAS\]](#), [Google Scholar](#) [open URL](#)

(b) Tachibana, Y.; Vayssieres, L.; Durrant, J. R. *Nat. Photonics* **2012**, 6, 511DOI: 10.1038/nphoton.2012.175

[\[Crossref\]](#), [\[CAS\]](#), [Google Scholar](#) [open URL](#)

(c) Gust, D.; Moore, T. A.; Moore, A. L. *Acc. Chem. Res.* **2009**, 42, 1890DOI: 10.1021/ar900209b



[\[ACS Full Text\]](#) , [\[CAS\]](#), [Google Scholar](#) [open URL](#)

---

4. 4

---

Suen, N. T.; Hung, S. F.; Quan, Q.; Zhang, N.; Xu, Y. J.; Chen, H. M. *Chem. Soc. Rev.* **2017**, 46, 337DOI: 10.1039/C6CS00328A

[\[Crossref\]](#), [\[PubMed\]](#), [\[CAS\]](#), [Google Scholar](#) [open URL](#)

---

5. 5

---

Karkas, M. D.; Verho, O.; Johnston, E. V.; Akermark, B. *Chem. Rev.* **2014**, 114, 11863DOI: 10.1021/cr400572f

[\[ACS Full Text\]](#) , [\[CAS\]](#), [Google Scholar](#) [open URL](#)

---

6. 6

---

Dismukes, G. C.; Brimblecombe, R.; Felton, G. A.; Pryadun, R. S.; Sheats, J. E.; Spiccia, L.; Swiegers, G. *F. Acc. Chem. Res.* **2009**, 42, 1935DOI: 10.1021/ar900249x

[\[ACS Full Text\]](#) , [\[CAS\]](#), [Google Scholar](#) [open URL](#)

---

7. 7

---

(a) Karkas, M. D.; Akermark, B. *Dalton Trans.* **2016**, 45, 14421DOI: 10.1039/C6DT00809G

[\[Crossref\]](#), [\[PubMed\]](#), [\[CAS\]](#), [Google Scholar](#) [open URL](#)

(b) Blakemore, J. D.; Crabtree, R. H.; Brudvig, G. W. *Chem. Rev.* **2015**, 115, 12974DOI: 10.1021/acs.chemrev.5b00122

[\[ACS Full Text\]](#) , [\[CAS\]](#), [Google Scholar](#) [open URL](#)

(c) Liu, X.; Wang, F. *Coord. Chem. Rev.* **2012**, 256, 1115DOI: 10.1016/j.ccr.2012.01.015

[\[Crossref\]](#), [\[CAS\]](#), [Google Scholar](#) [open URL](#)

---

8. 8

---

Thomsen, J. M.; Huang, D. L.; Crabtree, R. H.; Brudvig, G. W. *Dalton Trans.* **2015**, 44, 12452DOI: 10.1039/C5DT00863H

[\[Crossref\]](#), [\[PubMed\]](#), [\[CAS\]](#), [Google Scholar](#) [open URL](#)

---

9. 9

---

Tong, L.; Thummel, R. P. *Chem. Sci.* **2016**, 7, 6591DOI: 10.1039/C6SC02766K

[\[Crossref\]](#), [\[PubMed\]](#), [\[CAS\]](#), [Google Scholar](#) [open URL](#)

---

10. 10

---

(a) Duan, L.; Bozoglian, F.; Mandal, S.; Stewart, B.; Privalov, T.; Llobet, A.; Sun, L. *Nat. Chem.* **2012**, 4, 418DOI: 10.1038/nchem.1301

[\[Crossref\]](#), [\[PubMed\]](#), [\[CAS\]](#), [Google Scholar](#) [open URL](#)

(b) Duan, L.; Wang, L.; Li, F.; Li, F.; Sun, L. *Acc. Chem. Res.* **2015**, 48, 2084DOI: 10.1021/acs.accounts.5b00149


[\[ACS Full Text\]](#) , [\[CAS\]](#), [Google Scholar](#) [open URL](#)

---

11. 11

---

Duan, L.; Fischer, A.; Xu, Y.; Sun, L. *J. Am. Chem. Soc.* **2009**, 131, 10397DOI: 10.1021/ja9034686

[ACS Full Text](#) , [\[CAS\]](#), [Google Scholar](#) [open URL](#)

---

12. 12

---

(a) Clark, A. E.; Hurst, J. K. In *Mechanisms of Water Oxidation Catalyzed by Ruthenium Coordination Complexes*; Karlin, K. D., Eds.; Wiley: New York, **2012**.

[Google Scholar](#) [open URL](#)

(b) Shaffer, D. W.; Xie, Y.; Concepcion, J. J. *Chem. Soc. Rev.* **2017**, 46, 6170DOI: 10.1039/C7CS00542C

[\[Crossref\]](#), [\[PubMed\]](#), [\[CAS\]](#), [Google Scholar](#) [open URL](#)

---

13. 13

---

(a) Planas, N.; Vigara, L.; Cady, C.; Miro, P.; Huang, P.; Hammarstrom, L.; Styring, S.; Leidel, N.; Dau, H.; Haumann, M.; Gagliardi, L.; Cramer, C. J.; Llobet, A. *Inorg. Chem.* **2011**, 50, 11134DOI: 10.1021/ic201686c

[\[ACS Full Text\]](#) , [\[CAS\]](#), [Google Scholar](#) [open URL](#)

(b) Erdman, D.; Pineda-Galvan, Y.; Pushkar, Y. *Catalysts* **2017**, 7, 39DOI: 10.3390/catal7020039

[\[Crossref\]](#), [\[CAS\]](#), [Google Scholar](#) [open URL](#)

---

#### 14. 14

---


(a) Cape, J. L.; Lyman, S. V.; Lightbody, T.; Hurst, J. K. *Inorg. Chem.* **2009**, 48, 4400DOI: 10.1021/ic9001219

[\[ACS Full Text\]](#) , [\[CAS\]](#), [Google Scholar](#) [open URL](#)

(b) Moonshiram, D.; Alperovich, I.; Concepcion, J. J.; Meyer, T. J.; Pushkar, Y. *Proc. Natl. Acad. Sci. U. S. A.* **2013**, 110, 3765DOI: 10.1073/pnas.1222102110

[\[Free @ PNAS\]](#), [\[Crossref\]](#), [\[PubMed\]](#), [\[CAS\]](#), [Google Scholar](#) [open URL](#)

(c) Moonshiram, D.; Jurss, J. W.; Concepcion, J. J.; Zakharova, T.; Alperovich, I.; Meyer, T. J.; Pushkar, Y. J. *Am. Chem. Soc.* **2012**, 134, 4625DOI: 10.1021/ja208636f


[ACS Full Text](#) , [\[CAS\]](#), [Google Scholar](#) [open URL](#)

---

#### 15. 15

---

(a) Wasylenko, D. J.; Ganesamoorthy, C.; Henderson, M. A.; Koivisto, B. D.; Osthoff, H. D.; Berlinguette, C. *P. J. Am. Chem. Soc.* **2010**, 132, 16094DOI: 10.1021/ja106108y

[ACS Full Text](#) , [\[CAS\]](#), [Google Scholar](#) [open URL](#)

(b) Hughes, T. F.; Friesner, R. A. *J. Phys. Chem. B* **2011**, 115, 9280DOI: 10.1021/jp2026576

[\[ACS Full Text\]](#) , [\[CAS\]](#), [Google Scholar](#) [open URL](#)

(c) Masaoka, S.; Sakai, K. *Chem. Lett.* **2009**, 38, 182DOI: 10.1246/cl.2009.182


[\[Crossref\]](#), [\[CAS\]](#), [Google Scholar](#) [open URL](#)

---

#### 16. 16

---

(a) Pushkar, Y.; Moonshiram, D.; Purohit, V.; Yan, L.; Alperovich, I. J. *Am. Chem. Soc.* **2014**, 136, 11938DOI: 10.1021/ja506586b

[ACS Full Text](#) , [\[CAS\]](#), [Google Scholar](#) [open URL](#)

(b) Yan, L.; Zong, R.; Pushkar, Y. *J. Catal.* **2015**, 330, 255DOI: 10.1016/j.jcat.2015.07.018

[\[Crossref\]](#), [\[CAS\]](#), [Google Scholar](#) [open URL](#)

---

17. 17

---

Moonshiram, D.; Pineda-Galvan, Y.; Erdman, D.; Palenik, M.; Zong, R.; Thummel, R.; Pushkar, Y. J. *Am. Chem. Soc.* **2016**, 138, 15605DOI: 10.1021/jacs.6b08409

[ACS Full Text](#) , [\[CAS\]](#), [Google Scholar](#) [open URL](#)

---


18. 18

---

(a) Concepcion, J. J.; Tsai, M. K.; Muckerman, J. T.; Meyer, T. J. *J. Am. Chem. Soc.* **2010**, 132, 1545DOI: 10.1021/ja904906v

[ACS Full Text](#) , [\[CAS\]](#), [Google Scholar](#) [open URL](#)

(b) Wang, L. P.; Wu, Q.; Van Voorhis, T. *Inorg. Chem.* **2010**, 49, 4543DOI: 10.1021/ic100075k

[\[ACS Full Text\]](#) , [\[CAS\]](#), [Google Scholar](#) [open URL](#)

---

19. 19

---

Daniel, Q.; Huang, P.; Fan, T.; Wang, Y.; Duan, L.; Wang, L.; Li, F.; Rinkevicius, Z.; Mamedov, F.; Ahlquist, M. S. G.; Styring, S.; Sun, L. *Coord. Chem. Rev.* **2017**, 346, 206DOI: 10.1016/j.ccr.2017.02.019

[\[Crossref\]](#), [\[CAS\]](#), [Google Scholar](#) [open URL](#)

---

20. 20

---

Concepcion, J. J.; Zhong, D. K.; Szalda, D. J.; Muckerman, J. T.; Fujita, E. *Chem. Commun.* **2015**, 51, 4105DOI: 10.1039/C4CC07968J

[\[Crossref\]](#), [\[PubMed\]](#), [\[CAS\]](#), [Google Scholar](#) [open URL](#)

---

21. 21

---

(a) Bullock, R. M.; Das, A. K.; Appel, A. M. *Chem. - Eur. J.* **2017**, 23, 7626DOI: 10.1002/chem.201605066

[\[Crossref\]](#), [\[PubMed\]](#), [\[CAS\]](#), [Google Scholar](#) [open URL](#)

(b) Blanc, F.; Berthoud, R.; Coperet, C.; Lesage, A.; Emsley, L.; Singh, R.; Kreckmann, T.; Schrock, R. *R. Proc. Natl. Acad. Sci. U. S. A.* **2008**, 105, 12123DOI: 10.1073/pnas.0802147105

[\[Free @ PNAS\]](#), [\[Crossref\]](#), [\[PubMed\]](#), [\[CAS\]](#), [Google Scholar](#) [open URL](#)

(c) Coperet, C.; Comas-Vives, A.; Conley, M. P.; Estes, D. P.; Fedorov, A.; Mougél, V.; Nagae, H.; Nunez-Zarur, F.; Zhizhko, P. A. *Chem. Rev.* **2016**, 116, 323DOI: 10.1021/acs.chemrev.5b00373

[\[ACS Full Text\]](#) , [\[CAS\]](#), [Google Scholar](#) [open URL](#)

---

## 22. 22

(a) Sheridan, M. V.; Sherman, B. D.; Wee, K. R.; Marquard, S. L.; Gold, A. S.; Meyer, T. J. *Dalton Trans.* **2016**, 45, 6324DOI: 10.1039/C6DT00408C

[\[Crossref\]](#), [\[PubMed\]](#), [\[CAS\]](#), [Google Scholar](#) [open URL](#)

(b) Matheu, R.; Francàs, L.; Chernev, P.; Ertem, M. Z.; Batista, V.; Haumann, M.; Sala, X.; Llobet, A. *ACS Catal.* **2015**, 5, 3422DOI: 10.1021/acscatal.5b00132

[\[ACS Full Text\]](#) , [\[CAS\]](#), [Google Scholar](#) [open URL](#)

(c) Creus, J.; Matheu, R.; Penafiel, I.; Moonshiram, D.; Blondeau, P.; Benet-Buchholz, J.; Garcia-Anton, J.; Sala, X.; Godard, C.; Llobet, A. *Angew. Chem., Int. Ed.* **2016**, 55, 15382DOI: 10.1002/anie.201609167

[\[Crossref\]](#), [\[PubMed\]](#), [\[CAS\]](#), [Google Scholar](#) [open URL](#)

---

## 23. 23

(a) Sheridan, M. V.; Hill, D. J.; Sherman, B. D.; Wang, D.; Marquard, S. L.; Wee, K. R.; Cahoon, J. F.; Meyer, T. J. *Nano Lett.* **2017**, 17, 2440DOI: 10.1021/acs.nanolett.7b00105

[\[ACS Full Text\]](#) , [\[CAS\]](#), [Google Scholar](#) [open URL](#)

(b) Yamamoto, M.; Wang, L.; Li, F.; Fukushima, T.; Tanaka, K.; Sun, L.; Imahori, H. *Chem. Sci.* **2016**, 7, 1430DOI: 10.1039/C5SC03669K

[\[Crossref\]](#), [\[CAS\]](#), [Google Scholar](#) [open URL](#)

---

## 24. 24

Duan, L.; Araujo, C. M.; Ahlquist, M. S.; Sun, L. *Proc. Natl. Acad. Sci. U. S. A.* **2012**, 109, 15584DOI: 10.1073/pnas.1118347109

[\[Free @ PNAS\]](#), [\[Crossref\]](#), [\[PubMed\]](#), [\[CAS\]](#), [Google Scholar](#) [open URL](#)




25. 25

---

(a) Materna, K. L.; Crabtree, R. H.; Brudvig, G. W. *Chem. Soc. Rev.* **2017**, 46, 6099 DOI: 10.1039/C7CS00314E

[\[Crossref\]](#), [\[PubMed\]](#), [\[CAS\]](#), [Google Scholar](#) [open URL](#)

(b) Odrobina, J.; Scholz, J.; Risch, M.; Dechert, S.; Jooss, C.; Meyer, F. *ACS Catal.* **2017**, 7, 6235–6244 DOI: 10.1021/acscatal.7b01883

[\[ACS Full Text\]](#) , [\[CAS\]](#), [Google Scholar](#) [open URL](#)

---

26. 26

---

(a) Kröhnke, F. *Synthesis* **1976**, 1, 1 DOI: 10.1055/s-1976-23941

[\[Crossref\]](#), [Google Scholar](#) [open URL](#)

(b) Bozic-Weber, B.; Brauchli, S. Y.; Constable, E. C.; Fürer, S. O.; Housecroft, C. E.; Wright, I. A. *Phys. Chem. Chem. Phys.* **2013**, 15, 4500 DOI: 10.1039/c3cp50562f

[\[Crossref\]](#), [\[PubMed\]](#), [\[CAS\]](#), [Google Scholar](#) [open URL](#)

---

27. 27

---

Farnum, B. H.; Morseth, Z. A.; Brennaman, M. K.; Papanikolas, J. M.; Meyer, T. J. *J. Phys. Chem. B* **2015**, 119, 7698 DOI: 10.1021/jp512624u

[\[ACS Full Text\]](#) , [\[CAS\]](#), [Google Scholar](#) [open URL](#)

---

28. 28

---

Song, N.; Concepcion, J. J.; Binstead, R. A.; Rudd, J. A.; Vannucci, A. K.; Dares, C. J.; Coggins, M. K.; Meyer, T. J. *Proc. Natl. Acad. Sci. U. S. A.* **2015**, 112, 4935 DOI: 10.1073/pnas.1500245112

[\[Free @ PNAS\]](#), [\[Crossref\]](#), [\[PubMed\]](#), [\[CAS\]](#), [Google Scholar](#) [open URL](#)

---

29. 29

---

Schulze, M.; Kunz, V.; Frischmann, P. D.; Wurthner, F. *Nat. Chem.* **2016**, 8, 576 DOI: 10.1038/nchem.2503

[\[Crossref\]](#), [\[PubMed\]](#), [\[CAS\]](#), [Google Scholar](#) [open URL](#)

---

30. 30

---

Dengel, A. C.; Griffith, W. P. *Inorg. Chem.* **1991**, 30, 869DOI: 10.1021/ic00004a054

[\[ACS Full Text\]](#) , [\[CAS\]](#), [Google Scholar](#) [open URL](#)

---

31. 31

---

Dengel, A. C.; Griffith, W. P.; O'Mahoney, C. A.; Williams, D. J. J. *Chem. Soc., Chem. Commun.* **1989**, 22, 1720DOI: 10.1039/c39890001720


[\[Crossref\]](#), [Google Scholar](#) [open URL](#)

---

32. 32

---

Yano, J.; Robblee, J.; Pushkar, Y.; Marcus, M. A.; Bendix, J.; Workman, J. M.; Collins, T. J.; Solomon, E. I.; DeBeer George, S.; Yachandra, V. K. *J. Am. Chem. Soc.* **2007**, 129, 12989DOI: 10.1021/ja071286b

[ACS Full Text](#) , [\[CAS\]](#), [Google Scholar](#) [open URL](#)

---

33. 33

---

Lin, S.; Pineda-Galvan, Y.; Maza, W. A.; Epley, C. C.; Zhu, J.; Kessinger, M. C.; Pushkar, Y.; Morris, A. *J. ChemSusChem* **2017**, 10, 514DOI: 10.1002/cssc.201601181

[\[Crossref\]](#), [\[PubMed\]](#), [\[CAS\]](#), [Google Scholar](#) [open URL](#)

---

34. 34

---

Liu, Y.; Ng, S. M.; Lam, W. W.; Yiu, S. M.; Lau, T. C. *Angew. Chem., Int. Ed.* **2016**, 55, 288DOI: 10.1002/anie.201507933


[\[Crossref\]](#), [\[CAS\]](#), [Google Scholar](#) [open URL](#)

---

35. 35

---

Murakami, M.; Hong, D.; Suenobu, T.; Yamaguchi, S.; Ogura, T.; Fukuzumi, S. *J. Am. Chem. Soc.* **2011**, 133, 11605DOI: 10.1021/ja2024965

[ACS Full Text](#) , [\[CAS\]](#), [Google Scholar](#) [open URL](#)

---

36. 36

---

Shaffer, D. W.; Xie, Y.; Szalda, D. J.; Concepcion, J. J. J. Am. Chem. Soc. **2017**, 139, 15347DOI: 10.1021/jacs.7b06096

[ACS Full Text](#) , [\[CAS\]](#), [Google Scholar](#) [open URL](#)

---

37. 37

Ravel, B.; Newville, M. J. Synchrotron Radiat. **2005**, 12, 537DOI: 10.1107/S0909049505012719  
[\[Crossref\]](#), [\[PubMed\]](#), [\[CAS\]](#), [Google Scholar](#) [open URL](#)